JOURNAL OF VIROLOGY, June 2003, p. 6438–6449 Vol. 77, No. 11
0022-538X/03/$08.00+0 DOI: 10.1128/JVI.77.11.6438–6449.2003

The Oligomerization Domain of VP3, the Scaffolding Protein of Infectious Bursal Disease Virus, Plays a Critical Role in Capsid Assembly

Antonio Maraver,[1] Ana Oña,[1] Fernando Abaitua,[1] Dolores González,[1] Roberto Clemente,[1] Jose A. Ruiz-Díaz,[1] Jose R. Castón,[2] Florencio Pazos,[3] and Jose F. Rodriguez[1]*

Departments of Biología Molecular y Celular[1] and Estructura de Macromoléculas,[2] Centro Nacional de Biotecnología, Cantoblanco, 28049 Madrid, and Alma Bioinformática, Centro Empresarial Euronova, 28760 Tres Cantos, Madrid,[3] Spain

Received 1 November 2002/Accepted 6 March 2003

Infectious bursal disease virus (IBDV) capsids are formed by a single protein layer containing three polypeptides, pVP2, VP2, and VP3. Here, we show that the VP3 protein synthesized in insect cells, either after expression of the complete polyprotein or from a VP3 gene construct, is proteolytically degraded, leading to the accumulation of product lacking the 13 C-terminal residues. This finding led to identification of the VP3 oligomerization domain within a 24-amino-acid stretch near the C-terminal end of the polypeptide, partially overlapping the VP1 binding domain. Inactivation of the VP3 oligomerization domain, by either proteolysis or deletion of the polyprotein gene, abolishes viruslike particle formation. Formation of VP3-VP1 complexes in cells infected with a dual recombinant baculovirus simultaneously expressing the polyprotein and VP1 prevented VP3 proteolysis and led to efficient virus-like particle formation in insect cells.

The last four decades of the 20th century saw the emergence and global dispersion of a viral poultry disease known as infectious bursal disease. Infectious bursal disease is characterized by destruction of pre-B-lymphocyte populations residing within the bursa of Fabricius and the concomitant immunosuppression of affected birds (37). Infectious bursal disease is caused by infectious bursal disease virus (IBDV), a member of the *Birnaviridae* family (21). In spite of intensive vaccination programs with combinations of live and inactivated virus vaccines, infectious bursal disease outbreaks have been reported in all major poultry-producing countries (40).

IBDV particles are nonenveloped icosahedra with a diameter of 65 to 70 nm (4, 5). The capsid, formed by a single protein layer, exhibits a $T = 13$ symmetry, and it encloses a genome formed by two double-stranded RNA segments with a total coding capacity of approximately 3 kb. The major segment contains two partially overlapping open reading frames (ORFs). The first one codes for a 17-kDa polypeptide, VP5, that plays an important role in virus egress and virulence (24, 44). The second one codes for the virus polyprotein (105 kDa). The smaller segment contains a single ORF encoding the putative virus RNA-dependent RNA polymerase (RdRp), also known as VP1 (10).

The virus polyprotein, synthesized as a 105-kDa precursor, is cotranslationally cleaved to give three polypeptides known as pre-VP2 (pVP2; also known as VPX), VP4, and VP3, respectively. VP4, a new member of the lon family of proteases, is responsible for polyprotein cleavage (3). VP3 is a 29-kDa polypeptide that forms the trimeric subunits that wrap the inner surface of the capsid (4, 5). pVP2 undergoes a subsequent processing event to render a mature protein, VP2. The external surface of mature IBDV virions is formed by trimeric subunits containing a variable pVP2/VP2 ratio (6, 23). It has been suggested that pVP2→VP2 conversion is associated with the formation of mature capsids (6, 26). The cleavage sites for the proteolytic processing of the polyprotein and pVP2 have been characterized (9, 36), allowing faithful expression of the capsid polypeptides. The virus RdRp, VP1, interacts with VP3, forming a complex that facilitates VP1 encapsidation (23, 38). The VP3 domain responsible for this interaction is located at the 16 C-terminal residues of the protein (25). VP3 interacts with RNA in a sequence-independent fashion (19). It seems likely that, as is the case with inner capsid proteins from other viruses (15, 27, 31), VP3 might play a role in stabilizing the genomic RNA within the particle.

Heterologous expression vectors have been very useful to gather information about the structural and functional role of IBDV-encoded polypeptides (5, 6, 13, 14). Thus, it was shown that expression of the IBDV polyprotein from an inducible recombinant vaccinia virus (rVV) vector leads to formation of virus-like particles (VLPs). Despite the absence of the virus-encoded RdRp and double-stranded RNAs, VLPs are structurally identical to IBDV capsids (14). This demonstrated that correct IBDV capsid assembly does not require the expression of other virus-encoded polypeptides or the presence of the virus genome. Unexpectedly, polyprotein expression in insect cells with recombinant baculovirus (rBV) vectors leads to an extremely inefficient VLP assembly (6, 26). In particular, the use of FastBac-derived rBVs results in the exclusive assembly of large tubule-like structures formed by hexamers of pVP2 trimers (9, 26) identical to type I tubules isolated from IBDV-infected cells. It has been very recently shown that rBV-directed expression of a polyprotein chimera, containing the

* Corresponding author. Mailing address: Department of Biología Molecular y Celular, Centro Nacional de Biotecnología, Cantoblanco, 28049 Madrid, Spain. Phone: 34 91 5854558. Fax: 34 91 5854506. E-mail: jfrodrig@cnb.uam.es.

TABLE 1. Synthetic oligonucleotides used for the generation of His-VP3 carboxy-terminal end deletion mutants[a]

3′ primer	Sequence
His-VP3Δ248–257	CGC GGG TAC CTT ACC AGC GGC CCA GCC GAC C
His-VP3Δ243–257	CGC GGG TAC CTT AAC CAG GGG GTC TCT GTG TTG
His-VP3Δ238–257	CGC GGG TAC CTT ATG TTG GAG CAT TGG GTT TTG
His-VP3Δ233–257	CGC GGG TAC CTT ATT TTG GCT TGG GCT TTG G
His-VP3Δ228–257	CGC GGG TAC CTT ATG GTA GAG CCC GCC TGG G

[a] The 5′ primer was GGG GGA ATT CAT GGC ATC AGA GTT CAA AGA GAC CCC C.

heterologous green fluorescent protein (GFP) fused to the polyprotein C terminus, leads to VLP formation. However, the mechanism(s) underlying inefficient VLP assembly remained unknown (6).

In this report, we describe the results of a series of experiments aimed to shed light on this phenomenon. Data presented here demonstrates that inefficient VLP assembly in insect cells stems from the accumulation of a defective form of the inner capsid protein VP3, and that this can be prevented by coexpressing the virus-encoded RdRp, VP1. Most important, this investigation led to the identification of VP3 oligomerization as a fundamental step in IBDV capsid assembly. Here, we show for the first time that inactivation of the VP3 oligomerization domain completely abrogates VLP formation.

MATERIALS AND METHODS

Cells and viruses. rVVs VT7/VP3, and VT7/PolyΔ907-1012 have been previously described (13, 35). FB/Poly, FB/His-VP3 wild-type, FB/His-VP3Δ253-257, FB/His-VP3Δ1-25, FB/His-VP3Δ26-52, FB/His-VP3Δ53-77, FB/His-VP3Δ78-100, FB/His-VP3Δ101-124, FB/His-VP3Δ125-150, FB/His-VP3Δ151-175, FB/His-VP3Δ176-200, FB/His-VP3Δ201-224, and FB/His-VP3Δ216-257 have been previously described (19, 26). Expression experiments were carried out with either BSC-1 mammalian cells (American Type Culture Collection) for rVVs infections or *Trichoplusia ni* (H5) and *Spodoptera frugiperda* (Sf9) insect cells (Invitrogen) for rBVs. BSC-1 cells were grown in Dulbecco's modified Eagle's medium (DMEM) containing 10% newborn calf serum, and H5 and Sf9 cells were grown in TC-100 medium (Gibco-BRL) containing 10% fetal calf serum. rVVs, rBVs, and SalI IBDV strain adapted to grow in BSC-1 cells were grown and titrated as previously described (24, 26).

Construction of rBVs. The previously described plasmid pFB/His-VP3 wild-type (19), was used as template for the PCR synthesis of VP3-derived DNA fragments used in the construction of plasmids required for the generation of rBVs FB/His-VP3Δ248-257, FB/His-VP3Δ243-257, FB/His-VP3Δ238-257, FB/His-VP3Δ233-257, and FB/His-VP3Δ228-257, expressing His-VP3 C-terminal deletions. PCRs were carried out with a common 5′-end primer and a 3′-end primer specific for each mutant (see Table 1). After purification, PCR-derived DNA fragments were digested with *Apa*I and *Kpn*I and ligated to the plasmid pFB/His-VP3 (Gibco) previously digested with the same enzymes, giving rise the set of pFB/His-VP3 plasmids harboring the different His-VP3 C-terminal deleted genes under the control of the polyhedrin promoter.

Construction of plasmids required for the generation of rBVs FB/PolyΔ1008-1012, FB/PolyΔ1003-1012, and FB/PolyΔ998-1012 was achieved by substituting the *Xba*I fragment of pFB/Poly by the corresponding *Xba*I fragments obtained by digestion of plasmids FB/His-VP3Δ253-257, FB/His-VP3Δ248-257, and FB/His-VP3Δ243-257, respectively.

For the construction of plasmid pFB/VP1, the VP1 ORF of IBDV Soroa strain was isolated from the plasmid pBSKVP1 (23) by digestion with *Cla*I, followed by treatment with Klenow enzyme and a subsequent *Not*I digestion. The resulting fragment was subcloned into the pFastBac1 plasmid (Invitrogen) previously digested with *Stu*I and *Not*I, giving rise to plasmid pFB/VP1.

Dual rBV expression vectors pFBD/His-VP3-VP1 and pFBD/Poly-VP1 were constructed by inserting the His-VP3 and the polyprotein ORFs, respectively, into the plasmid pFBD/VP1. pFBD/VP1 was generated by inserting a DNA fragment generated by digestion of the plasmid pBSKVP1 with *Not*I, followed by treatment with Klenow enzyme, and subsequent *Xho*I digestion. This fragment was subcloned into the pFastBacDual plasmid (Invitrogen) previously digested with *Xho*I and *Pvu*II. Thereafter, the plasmid pFB/His-VP3 (19) was digested with *Not*I and *Rsr*II. The resulting fragment was ligated to the plasmid pFBD/VP1 previously digested with the same enzymes, giving rise to the plasmid pFBD/His-VP3-VP1. Similarly, the polyprotein gene was isolated from the plasmid pCIneoPoly (25) by digestion with *Eco*RI and *Not*I. The resulting fragment was subcloned into pFBD/VP1 plasmid previously digested with the same enzymes, giving rise the plasmid pFBD/Poly-VP1.

rBVs expressing the constructs described above were generated with the Bac-to-Bac system following the manufacturers instructions (Invitrogen BV, Groningen, The Netherlands).

Characterization and purification of polyprotein-derived structures by sucrose gradient sedimentation. BSC-1 or H5 cells were infected with rVV or rBV at a multiplicity of infection of 5 PFU/cell. Infected cells were harvested, lysed, and processed as described previously (23, 26).

Electron microscopy analysis. Samples (5 μl) obtained from sucrose gradient sedimentation of cell lysates were applied to glow-discharged carbon-coated grids for 1-2 min, and negatively stained with 2% aqueous uranyl acetate for 1 min. Micrographs were recorded with a Jeol 1200 EXII electron microscope operating at 100 kV at a nominal magnification of either 20,000× or 40,000×.

IMAC purification of His-VP3 fusion proteins. H5 or Sf9 cells were infected with rBVs at a multiplicity of infection of 5 PFU/cell. Cells were harvested at 72 h postinfection and washed twice with phosphate-buffered saline. Cell pellets were then resuspended in lysis buffer (50 mM Tris-HCl, pH 8.0; 500 mM NaCl) supplemented with protease inhibitors (Complete Mini; Roche) and maintained on ice for 20 min. Thereafter, extracts were centrifuged 13,000 × *g* for 10 min at 4°C. The supernatant was collected and subjected to Metal affinity chromatography (IMAC) purification with a cobalt-based resin (Talon, Clontech Laboratories, Inc., Palo Alto, Calif.) following the protocol described by the manufacturers.

PAGE and Western blot analysis. Protein samples were resuspended in Laemmli's sample buffer and heated at 100°C for 5 min. Electrophoreses were carried out with 11% polyacrylamide gels. For Western blot analyses, after electrophoresis, proteins were electroblotted onto Hybond-C nitrocellulose membranes. Before incubation with specific antisera, membranes were blocked by incubation with 5% nonfat dry milk in phosphate-buffered saline for 1 h at room temperature.

Immunofluorescence and confocal laser scanning microscopy analysis. BSC-1 and H5 cells seeded onto glass coverslips were infected with rVVs or rBVs at a multiplicity of infection of 1 PFU/cell. Cells were washed twice with phosphate-buffered saline at 24 h postinfection in rVV assays and 72 h postinfection in H5 assays and then fixed in methanol at −20°C for 10 min. After fixation, coverslips were air-dried, blocked in phosphate-buffered saline containing 20% normal calf serum for 1 h and incubated with the indicated antisera diluted in phosphate-buffered saline supplemented with 5% NCS for 45 min at room temperature. Immunoglobulin G was visualized with either goat anti-rat immunoglobulin antibodies conjugated to Alexa 594 or with goat anti-rabbit immunoglobulin antibodies conjugated to Alexa 488 (Jackson ImmunoResearch Laboratories Inc.). Coverslips were dehydrated with ethanol, mounted, and visualized by epifluorescence with a Zeiss Axiovert 200 microscope equipped with a Bio-Rad Radiance 2100 confocal system. Images were captured with the Laser Sharp software package (Bio-Rad).

Mass spectrometry analysis. IMAC-purified His-VP3 polypeptides were passed through C-18 ZipTip tips (Millipore, Bedford, Mass.), and the eluted proteins were mixed 1:1 with matrix solution (saturated 3,5-dimethoxy-4-hydroxycinnamic acid in 33% aqueous acetonitrile and 0.1% trifluoroacetic acid). A 0.7-μl aliquot of this mixture was deposited onto a stainless steel matrix-assisted laser desorption ionization probe and allowed to dry at room temperature. Samples were measured on a Bruker Reflex IV matrix-assisted laser desorption ionization-time of flight-mass spectrometry (MALDI-TOF) mass spectrometer (Bruker-Franzen Analytic GmbH, Bremen, Germany) equipped with the SCOUT source in positive ion reflector mode with delayed extraction. The ion acceleration voltage was 20 kV. The equipment was externally calibrated by employing protonated mass signals from bovine serum albumin and bovine serum albumin dimer covering the 20 to 130 *m*/*z* range.

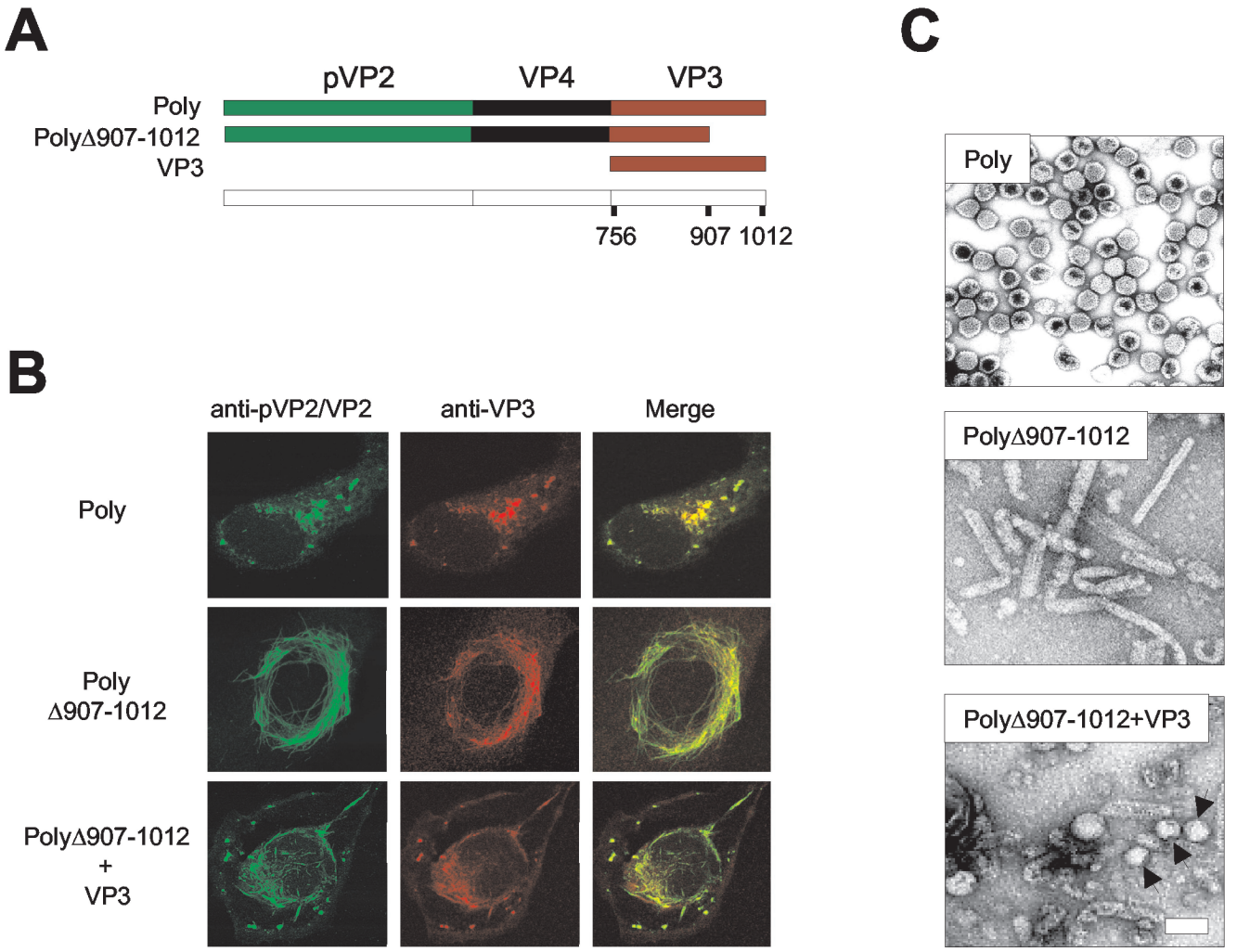

FIG. 1. Effect of VP3 C-terminal deletion on VLP morphogenesis. (A) The diagram depicts the IBDV-derived genes expressed by the different rVVs used to test the effect of the VP3 C-terminal deletion on VLP formation in mammalian cells. VT7/Poly expresses the wild-type polyprotein. VT7/PolyΔ907-1012 expresses a deleted form of the polyprotein lacking the 105 C-terminal residues. VT7/VP3 expresses full-length VP3. (B) Effect of VP3 C-terminal deletion on pVP2/VP2 subcellular distribution. Digital confocal images of cells infected with VT7/Poly pr VT7/PolyΔ907-1012 or coinfected with VT7/PolyΔ907-1012 and VT7/VP3. At 24 h postinfection, cells were fixed and incubated with rabbit anti-pVP2/VP2 and rat anti-VP3, followed by incubation with goat anti-rabbit immunoglobulin coupled to Alexa 488 (green) and goat anti-rat immunoglobulin coupled to Alexa 594 (red). (C) Effect of VP3 C-terminal deletion on VLP assembly. Extracts from cells infected with VT7/Poly or VT7/PolyΔ907-1012 or coinfected with VT7/PolyΔ907-1012 and VT7/VP3 were subjected to sucrose gradient fractionation. Fractions were spotted onto a carbon-filmed grid, negatively stained, and visualized by electron microscopy. The images represent assemblies detected in equivalent fractions from the three samples.

Protein structure prediction. Two secondary-structure prediction systems were used through their public web interfaces: PROF (the new version of PHD) (33) and PsiPred (16). The search for "low complexity regions" was performed with the SEG program (42) included in the Blast package (1). The Agadir algorithm (20) was used to predict the helical propensity of peptides. Natively unstructured (disordered) regions were predicted with the PONDR system (22).

RESULTS

Deletion of VP3 C-terminal end abolishes VLP assembly. We have recently demonstrated that the VP3 C-terminal end contains the motif responsible for the interaction with VP1 (25). We sought to characterize the role of the VP3 C-terminal region on VLP morphogenesis. As a starting point for this study, an rVV, VT7/PolyΔ907-1012, expressing a deleted form of the polyprotein lacking the 105 C-terminal VP3 residues was used (35) (Fig. 1A). Sodium dodecyl sulfate-polyacrylamide gel electrophoresis (SDS-PAGE) analysis of extracts from metabolically labeled BSC-1 cells infected with VT7/PolyΔ907-1012 showed that the deletion does not affect the cotranslational processing of the polyprotein (35). Interestingly, expression of PolyΔ907-1012 leads to accumulation of tubule-like structures akin to type I tubules found in IBDV-infected cells (18). PolyΔ907-1012-derived type I tubular assemblies were detectable by immunofluorescence with both anti-pVP2/VP2 and anti-VP3 sera (Fig. 1B) and by electron microscopy analysis of fractions from sucrose gradients (Fig. 1C).

To confirm whether the observed phenotype was the result of the VP3 deletion, an experiment was carried out by coin-

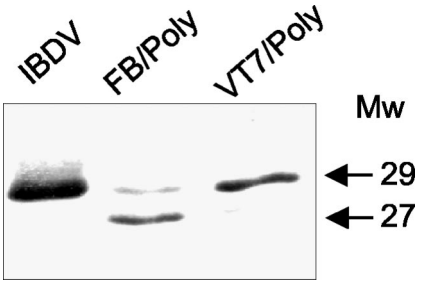

FIG. 2. Comparative Western blot analysis of VP3 expressed in different systems. Extracts from IBDV-, VT7/Poly-, and FB/Poly-infected cells were subjected to SDS-PAGE and Western blot analysis with rabbit anti-VP3 serum, followed by addition of horseradish peroxidase-conjugated goat anti-rat immunoglobulin. Signal was detected by enhanced chemiluminescence. The position and molecular masses (in kilodaltons) of the immunoreactive VP3 bands are indicated.

fecting BSC-1 cells with VT7/PolyΔ907-1012 and VT7/VP3. The latter, a previously described rVV (13), expresses wild-type VP3. Confocal laser scanning microscopy analysis of infected cells showed that coexpression of wild-type VP3 strongly reduced the formation of type I tubules. In coinfected cells, the pVP2/VP3 distribution was characterized by the formation of short tubules and viroplasms similar to those observed in cells infected with the wild-type polyprotein (Fig. 1B). This observation indicated that coexpression of wild-type VP3 partially rescues the ability of PolyΔ907-1012 to form VLPs. Electron microscopy analysis of sucrose gradient fractions from coinfected cells confirmed this hypothesis. The top fractions of the gradient were highly enriched in short tubules and quasi-spherical assemblies (capsoids) with a diameter of 60 to 70 nm, along with a small proportion of VLPs with a polygonal contour (Fig. 1C). These results showed that the VP3 C terminus plays a critical role during IBDV morphogenesis.

VP3 is proteolytically processed in insect cells. It has been previously described that expression of the IBDV polyprotein in insect cells leads to the assembly of large tubules formed by hexamers of pVP2 trimers (9, 26). The similarity between rBV- and PolyΔ907-1012-derived tubules prompted a careful analysis of the VP3 expressed in insect cells. The previously described FB/Poly (26), expressing the full-length polyprotein, was used for this study. Extracts from cells infected with IBDV, VT7/Poly, and FB/Poly were analyzed by Western blot with anti-VP3 serum (13). A single 29-kDa band, corresponding to the expected size of VP3, was detected in samples from IBDV- and VT7/Poly-infected cells (Fig. 2). In contrast, two bands of 29 and 27 kDa were found in the sample from H5 cells infected with FB/Poly (Fig. 2). A time course expression analysis showed that, although the appearance of the 27-kDa band was slightly delayed with respect to the 29-kDa product, it became highly predominant later during the infection (see Fig. 8A). A similar analysis was performed with Sf9 cells. The results obtained were identical to those described above. These results showed that, in insect cells, VP3 undergoes a posttranslational modification that results in the accumulation of a 27-kDa product.

Infection of H5 cells with an rBV expressing an N-terminally six-histidine-tagged version of VP3 (Fig. 3A), FB/His-VP3, resulted in the accumulation of two VP3-immunoreactive

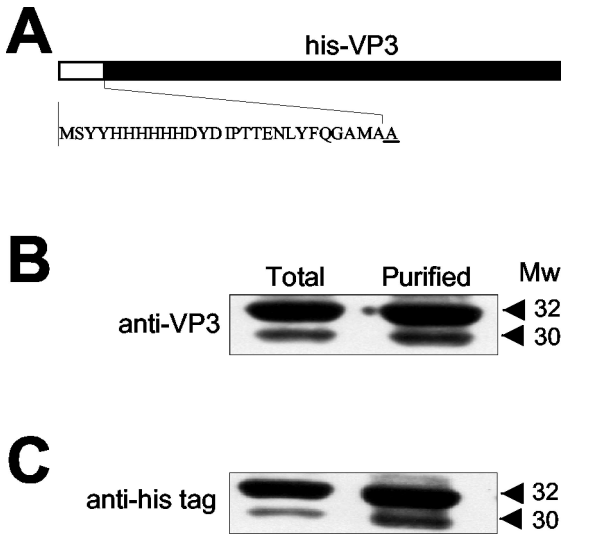

FIG. 3. Characterization of proteolytic trimming of VP3 expressed in insect cells. (A) Diagram depicting the N-terminally His-tagged VP3 fusion gene expressed by the rBV FB/His-VP3. The sequence corresponding to the six-histidine tag and the first VP3 residue (underlined) is shown. Samples from total FB/His-VP3 H5-infected cells and affinity-purified His-VP3 were subjected to SDS-PAGE and Western blot analysis with anti-VP3 (B) and anti-His tag (C) sera, followed by addition of horseradish peroxidase-conjugated goat anti-rat immunoglobulin. The signal was detected by enhanced chemiluminescence. The positions and estimated molecular masses (in kilodaltons) of the immunoreactive bands are indicated.

bands akin to those observed in cells infected with FB/Poly (19). We used FB/His-VP3 in order to characterize the origin of the smaller VP3 product. Total cell extracts and IMAC-purified His-VP3 were subjected to SDS-PAGE followed by Western blot analysis. As shown in Fig. 3, the 32- and 30-kDa products were specifically recognized by anti-VP3 (Fig. 3B) and by the anti-His tag (Fig. 3C) sera, respectively, indicating that the N-terminal histidine tag remained intact. These results strongly suggested that, in insect cells, VP3 is proteolytically trimmed, giving rise to a polypeptide lacking a 2-kDa fragment from its C-terminal end.

In order to firmly establish whether the formation of the smaller VP3 product was the result of a C-terminal proteolytic trimming, six rBVs, His-VP3Δ253-257, His-VP3Δ248-257, His-VP3Δ243-257, His-VP3Δ238-257, His-VP3Δ233-257, and His-VP3Δ228-257, were used. These rBVs express N-terminal six-histidine-tagged VP3 polypeptides containing a series of five-amino-acid-long stepwise C-terminal deletions (see Fig. 4A). VP3 expression was then analyzed by Western blot of extracts from rBV-infected H5 cells with VP3 antiserum. As shown in Fig. 4B, expression of both wild-type His-VP3 and His-VP3Δ253-257 rendered VP3 doublets. Mutant proteins containing deletions of 10 or more residues migrated according to their predicted sizes, giving rise to single VP3 bands (Fig. 4B). This result demonstrates that the C-terminal end of VP3 is proteolytically cleaved and that deletion of the cleavage site prevents the trimming. It is noteworthy that the mobility of His-VP3Δ248-257 was slightly slower than that of the polypeptides produced by cleavage of His-VP3 and His-VP3Δ253-257. This indicated that processing takes place within the stretch

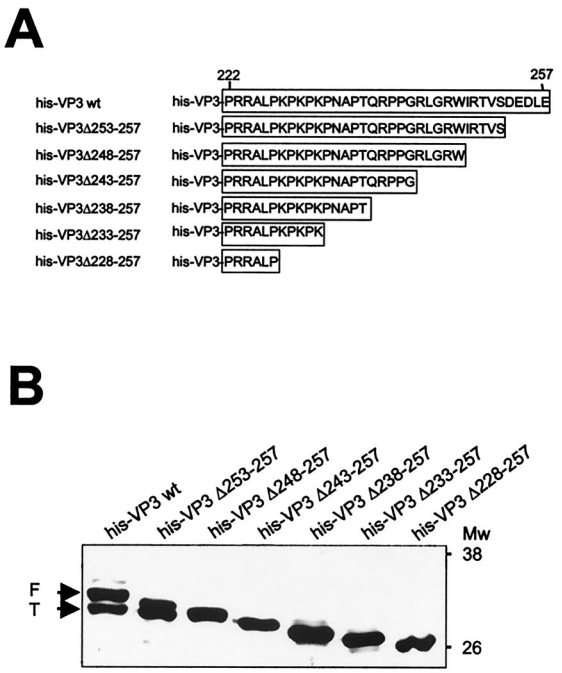

FIG. 4. Mapping VP3 proteolytic cleavage site. (A) The diagram shows the set of VP3 C-terminal deletion mutants used for mapping the VP3 cleavage site. (B) Western blot analysis of IMAC-purified polypeptides encoded by the different VP3 C-terminal deletion mutants. Extracts from rBV-infected cells were subjected to IMAC. Affinity-purified polypeptides were subjected to SDS-PAGE and Western blot analysis with rabbit anti-VP3 serum, followed by addition of horseradish peroxidase-conjugated goat anti-rat immunoglobulin. The signal was detected by enhanced chemiluminescence. The positions of molecular mass markers are shown (in kilodaltons). Arrows indicate the position corresponding to full-length (F) and C-terminally trimmed (T) His-VP3 polypeptide products.

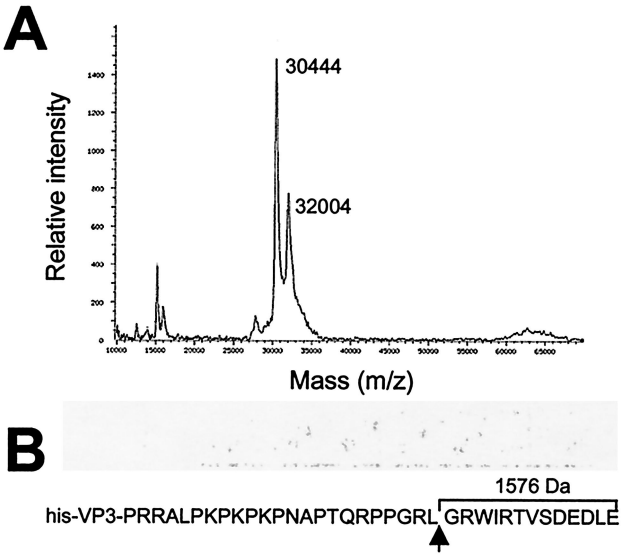

FIG. 5. Determination of molecular masses of affinity-purified His-VP3 polypeptides. (A) Mass spectrum of proteins recovered after affinity purification of extracts from FB/His-VP3-infected H5 cells. The sample was analyzed with a MALDI-TOF mass spectrometer. The molecular masses corresponding to the full-length and C-terminally trimmed VP3 products are indicated. (B) The diagram shows the sequence corresponding to the VP3 C-terminal end. The position of the VP3 proteolytic cleavage site (arrow) and the molecular mass of the 13-amino-acid peptide released by proteolytic cleavage are indicated.

located between residues 243 and 248. Most likely, the C-terminal end of His-VP3Δ248-257 is too short to allow recognition of the cleavage site by the responsible protease(s), thus precluding its cleavage.

To confirm the results obtained with the deletion mutants, and to precisely establish the position of the VP3 cleavage site, extracts from BV/His-VP3-infected H5 cells were subjected to IMAC purification and analyzed by mass spectrometry. The experiment was repeated three times with independent IMAC purifications. The results obtained were almost identical in all cases (less than 0.03% mass difference). Figure 5A shows the results of one such experiment. Two polypeptides of 32,004 and 30,444 Da were detected, indicating that proteolytic processing removes a peptide of 1,560 Da from the VP3 C terminus. This value matches the predicted size (1,576 Da) of the 13-amino-acid VP3 C-terminal peptide 245GRWIRTVSDE DLE257.

Taken together, these results demonstrate that VP3 is cleaved between residues L244 and G245, rendering a polypeptide lacking the 13 C-terminal residues.

Coexpression of VP1 prevents C-terminal trimming of VP3. The formation of VP3-VP1 complexes requires the presence of the 16-amino-acid C-terminal tail of VP3 (25). Even more, the fusion of this 16-amino-acid peptide, designated the VP1 binding motif, to the heterologous GFP protein was enough to confer the ability to bind VP1 in vitro (25) on this GFP chimera. Hence, it seemed feasible that formation of VP3-VP1 complexes might hamper the access of the protease to the VP3 cleavage site and thus prevent proteolysis. To analyze this hypothesis, a dual rBV, FBD/His-VP3-VP1, expressing both the His-VP3 and VP1 genes, was generated. IMAC purification of FB/His-VP3-infected cells extracts gave a 32- to 30-kDa VP3 doublet as well as three additional, much fainter bands of approximately 60, 70, and 95 kDa (Fig. 6A).

IMAC purification of a sample from FBD/His-VP3-VP1-infected cells gave two bands corresponding to His-VP3 and VP1 as well as the three dim bands described above (Fig. 6). This showed that VP3-VP1 complexes are efficiently formed in insect cells. Interestingly, in these samples, the band corresponding to the C-terminally trimmed His-VP3 was barely detectable, indicating that VP1 coexpression prevents proteolysis. To further characterize this finding, a comparative analysis of the His-VP3 profiles obtained after IMAC purification of samples from cells infected with FB/His-VP3 or FBD/His-VP3-VP1 or coinfected with FB/His-VP3 and FB/VP1 was carried out. As shown in Fig. 6B, while most of the detectable VP3 in the sample from FB/His-VP3 corresponded to the proteolytically trimmed species, this polypeptide was almost undetectable in samples from cells coinfected with FB/His-VP3 and FB-VP1 or infected with FBD/His-VP3-VP1. These results demonstrate that formation of VP3-VP1 complexes efficiently blocks VP3 proteolytic cleavage.

VP3 oligomerization domain mapping. The use of a yeast two-hybrid expression system showed that VP3 is able to form

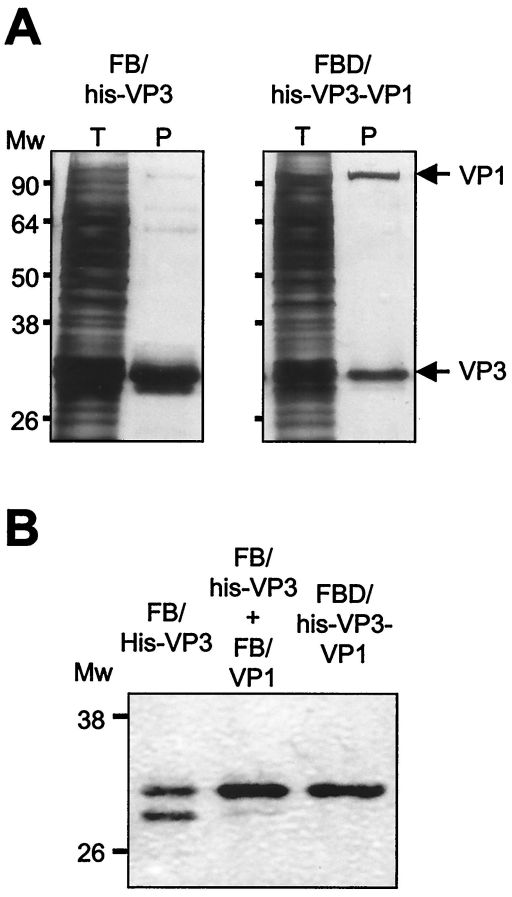

FIG. 6. Effect of VP1 coexpression on His-VP3 proteolytic cleavage. (A) Detection of VP3-VP1 complexes. H5 cells were infected with FB/His-VP3 or FB/His-VP3-VP1. At 72 h postinfection, cells were harvested, and the corresponding extracts were subjected to IMAC purification. Samples corresponding to total cell extracts (T) and IMAC-purified polypeptides (P) were analyzed by SDS-PAGE. After electrophoresis, gels were fixed and silver stained. The positions of molecular mass markers are indicated (in kilodaltons). (B) Western blot analysis of extracts from H5 cells infected with FB/His-VP3 or FB/His-VP3-VP1 or coinfected with FB/His-VP3 and FB/His-VP1. Infected cells were harvested at 72 h postinfection, resuspended in lysis buffer, and subjected to IMAC purification. Samples were subjected to SDS-PAGE and Western blot analysis with rabbit anti-VP3 serum, followed by addition of horseradish peroxidase-conjugated goat anti-rat immunoglobulin. The signal was detected by enhanced chemiluminescence. The positions of molecular mass markers (in kilodaltons) are indicated.

self-complexes (38). We have consistently observed the presence of a ladder of high-molecular-mass protein bands, ranging from 65 to 170 kDa, in IMAC-purified wild-type His-VP3 samples (see Fig. 6A and 7B and C), indicating the existence of VP3 oligomers resistant to denaturation.

In order to further assess the formation of His-VP3 oligomers, a previously described (19) set of 10 rBVs expressing His-VP3 deletion mutants was used. These mutants harbor deletions of 25 to 42 amino acids spanning the complete VP3 sequence (Fig. 7A). The different proteins were expressed in H5 cells, subjected to IMAC purification, and analyzed by SDS-PAGE and Western blot with anti-VP3 serum. As shown in Fig. 7B, with the exception of only His-VP3Δ216-257, high-molecular-mass VP3 ladders were detected in samples from all mutants. This indicated that the domain responsible for the formation of VP3 oligomers maps within the 42 C-terminal residues of the polypeptide. In addition to this, analysis of the migration patterns observed with the different mutants in relation to the masses of their corresponding monomers, indicated that the high-molecular-mass VP3 bands observed in the sample from wild-type His-VP3 might correspond to dimers (60 to 70 kDa), trimers (85 to 90 kDa), and hexamers (160 to 170 kDa).

To obtain a more refined map of the VP3 oligomerization domain, the set of His-VP3 C-terminal deletion mutants described above (see Fig. 4) was used. The different proteins were IMAC purified and subjected to SDS-PAGE. After electrophoresis, the gels were subjected to Western blot analysis with anti-VP3 serum. Overexposure of the Western blots showed the presence of VP3 oligomeric forms in the samples corresponding to the wild-type His-VP3, His-VP3Δ253-257, and His-VP3Δ248-257 polypeptides (Fig. 7C). This pattern was not detected in samples from the rest of the mutants containing larger deletions.

Coexpression of VP1 leads to efficient VLP assembly in insect cells. The finding that the VP3 C-terminal tail is involved in oligomerization suggested that it might play a critical role in VLP assembly. Accordingly, a blockade of the observed VP3 C-terminal proteolytic processing might lead to VLP formation in insect cells. To analyze this hypothesis, a dual rBV, FBD/Poly-VP1, simultaneously expressing the polyprotein and the VP1 genes, was generated. A VP3 time course expression analysis was carried out with cells infected with FB/Poly and FBD/Poly-VP1. In agreement with previous results, expression in FB/Poly-infected cells gave a VP3 doublet (Fig. 8A). The band corresponding to full-length VP3 constituted a rather small fraction of the total VP3 detected in samples collected at 48 h and later times postinfection. A completely different situation was found in samples from FBD/Poly-VP1-infected cells, in which intact VP3 constituted the large majority of the total VP3 detected at all times postinfection. This shows that the VP3 generated by polyprotein expression is also protected against proteolysis by the presence of VP1.

A confocal laser scanning microscopy analysis was performed to determine the effect of VP1 coexpression on the subcellular distribution of the structural proteins pVP2/VP2 and VP3. H5 cells were infected with either FB/Poly or FBD/Poly-VP1. At 72 h postinfection, cells were fixed and incubated with anti-pVP2/VP2 and -VP3 antisera. As shown in Fig. 8B, pVP2/VP2 and VP3 expressed in FB/Poly-infected cells gave rise to large tubular structures containing both proteins. This pattern was also observed in cells infected with FBD/Poly-VP1. In addition to the tubular structures, these cells contained viroplasm-like accumulations formed by both proteins, similar to those found in IBDV-infected cells (24). This observation indicated that VP1 expression modifies the assembly of the IBDV capsid proteins expressed in insect cells.

To analyze the IBDV-derived structures generated in these cells, extracts from FB/Poly- and FBD/Poly-VP1-infected cells were subjected to centrifugation in 25 to 50% sucrose gradients. The fractions collected from these gradients were negatively stained and analyzed by transmission electron micros-

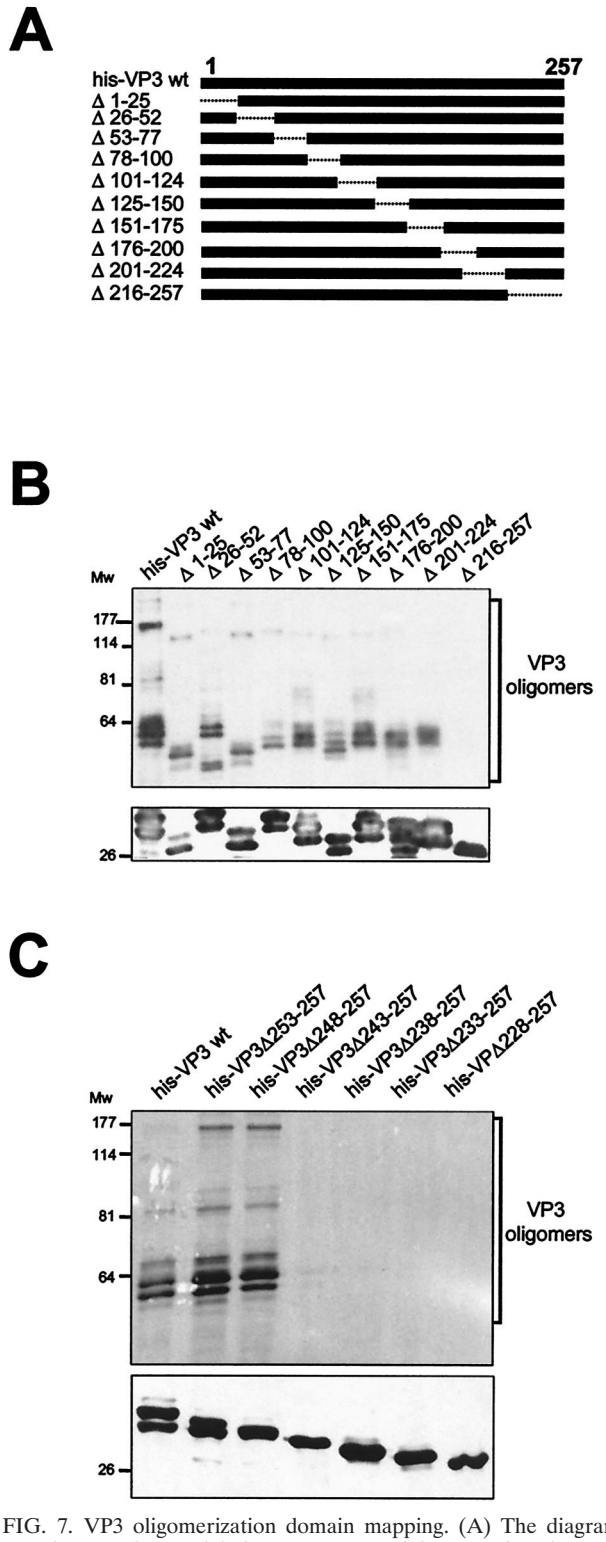

FIG. 7. VP3 oligomerization domain mapping. (A) The diagram shows the set of VP3 deletion mutants used for mapping the VP3 oligomerization domain. Deleted regions are depicted as dashed lines. The name of each mutant refers to the boundaries of the deleted region. (B) Detection of VP3 oligomers. His-VP3 proteins were affinity purified, subjected to SDS-PAGE and Western blot analysis with rabbit anti-VP3 serum, followed by addition of horseradish peroxidase-conjugated goat anti-rat immunoglobulin. The signal was detected by enhanced chemiluminescence. Blots were excised, and the upper half was overdeveloped to facilitate the detection of oligomers. The lower half, containing His-VP3 monomers, was developed with a shorter exposure. The positions of molecular mass markers (in kilodaltons) are indicated. (C) Detection of VP3 oligomers produced by C-terminal His-VP3 deletion mutant proteins. Proteins were affinity purified, subjected to SDS-PAGE and Western blot analysis with rabbit anti-VP3 serum, followed by addition of horseradish peroxidase-conjugated goat anti-rat immunoglobulin. The signal was detected by enhanced chemiluminescence. Blots were excised, and the upper half was overdeveloped to facilitate the detection of oligomers. The lower half of the blot, containing His-VP3 monomers, was developed with a shorter exposure time. The positions of molecular mass markers (in kilodaltons) are indicated.

copy. As has been described previously (26), most of the material from FB/Poly-infected cells was found at the bottom of the gradient. This material consisted mostly of large, rigid tubules identical to type I IBDV tubules (Fig. 9A). Although a small amount of rigid tubules was detected in the bottom fractions, most of the material found in FBD/Poly-VP1-derived gradients was found at the upper fractions (Fig. 9A). Analysis of the top fractions of this gradient showed the presence of abundant VLPs 65 to 70 nm in diameter and with a polygonal morphology identical to that of IBDV virions (Fig. 9B).

Fractions corresponding to the top of these gradients were analyzed by Western blot with anti-VP1, -pVP2/VP2, and -VP3 sera. As expected, the presence of VP1 was only detected in the sample corresponding to FBD/Poly-VP1-infected cells (Fig. 9C). The anti-pVP2/VP2 serum revealed the presence of pVP2 in both samples. Interestingly, VP2 was only detected in the sample corresponding to FBD/Poly-VP1-infected cells. Finally, as expected, the full-length/trimmed VP3 ratio was much higher in the sample from FBD/Poly-VP1-infected cells than in its counterpart from cells infected with FB/Poly. These results demonstrate that VP1 modifies pVP2/VP2-VP3 assembly leading to the formation of bona fide VLPs containing the structural polypeptides (VP1, pVP2/VP2, and VP3) found in purified IBDV virions.

The results shown in Fig. 8A raised the interesting possibility that VLPs might be present in cells infected with FB/Poly at 24 h postinfection, while most of the VP3 polypeptide remains intact. However, attempts to purify VLPs at 24 h postinfection from cells infected with either FB/Poly or FBD/Poly-VP1 were unsuccessful (data not shown). Failure to recover VLPs probably reflects the relatively low intracellular concentration of pVP2 and VP3 at this time postinfection.

In view of these results, and knowing that His-VP3 mutants lacking 5 or 10 C-terminal residues formed oligomers, it was interesting to explore whether expression of polyproteins harboring 5- and 10-amino-acid C-terminal deletions in VP3 resulted in the formation of VLPs. Three rBVs, FB/PolyΔ1008-1012, FB/PolyΔ1003-1012, and FB/PolyΔ998-1012, containing deletions identical to those found in mutants His-VP3Δ253-257, His-VP3Δ248-257, and His-VP3Δ243-257, respectively, were constructed (see Fig. 4A) but within the context of the whole polyprotein. As expected, expression of FB/PolyΔ1008-1012 rendered a 28- and 27-kDa VP3 doublet (data not shown). Cells infected with FB/PolyΔ1003-1012, and FB/PolyΔ998-1012 accumulated single VP3 polypeptides of 27, and 26 kDa, respectively (data not shown), confirming the data

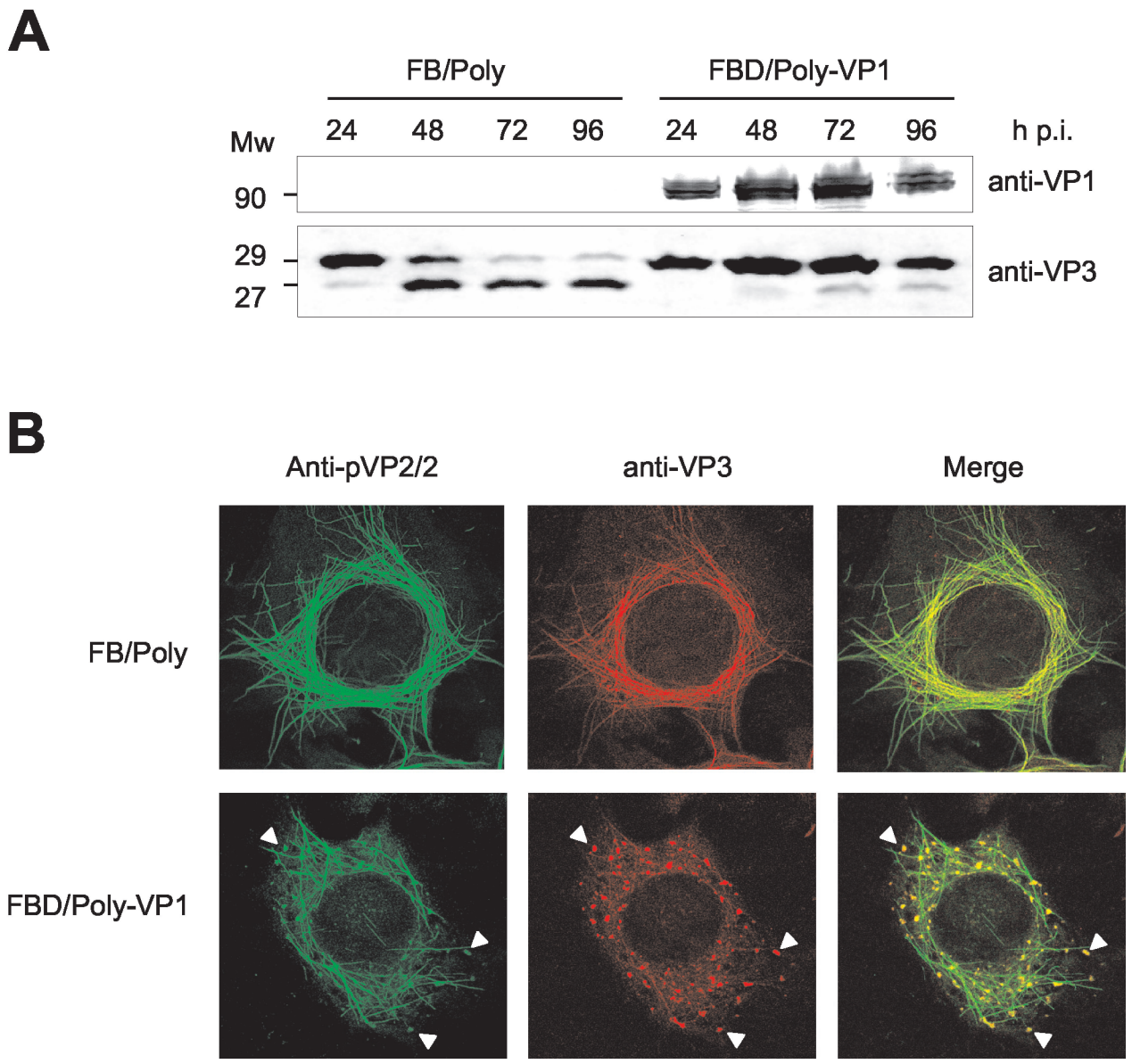

FIG. 8. Characterization of effect of VP1 coexpression on VP3 proteolytic processing and subcellular distribution of capsid proteins. (A) Detection of VP1 and VP3 polypeptides that accumulated in FB/Poly- and FBD/Poly-VP1-infected cells. Infected cells were harvested at 24, 48, 72, and 96 h postinfection. The samples were analyzed by Western blot with anti-VP1 and -VP3 sera, followed by addition of horseradish peroxidase-conjugated goat anti-rat immunoglobulin. The signal was detected by enhanced chemiluminescence. The position of molecular mass markers (in kilodaltons) are indicated. (B) The subcellular distribution of pVP2/VP2 and VP3 polypeptides in cells infected with FB/Poly and FBD/Poly-VP1 was analyzed by confocal laser scanning microscopy. At 60 h postinfection, cells were fixed and incubated with rabbit anti-pVP2/VP2 and rat anti-VP3, followed by incubation with goat anti-rabbit immunoglobulin coupled to Alexa 488 (green) and goat anti-rat immunoglobulin coupled to Alexa 594 (red). Arrowheads indicate the positions of viroplasm-like areas containing pVP2/VP2 and VP3.

obtained with the His-VP3 deletion mutants (Fig. 4B). Attempts to detect the formation of either viroplasms, by confocal laser scanning microscopy, or VLPs, by sucrose gradient fractionation, were unsuccessful (data not shown), indicating that deletion of five or more C-terminal VP3 residues completely abolishes VLP morphogenesis. Additionally, attempts to generate VLPs by VP1 coexpression with these mutants also failed. This was expected because removal of the five C-terminal VP3 residues completely abolishes VP3-VP1 complex formation (25).

VP3 structural predictions. The availability of a three-dimensional structural model for VP3 would facilitate a better understanding of some of the results described above. So far, our attempts to obtain VP3 crystals in order to facilitate X-ray analyses have failed. To partially overcome this problem, we have performed a computing analysis to gather information about the possible VP3 secondary structure. All the secondary-structure prediction programs used agree that VP3 is an all-α protein (8 to 10 α). Only a small signal of β is detected around position 135 but with low reliability. Secondary-structure pre-

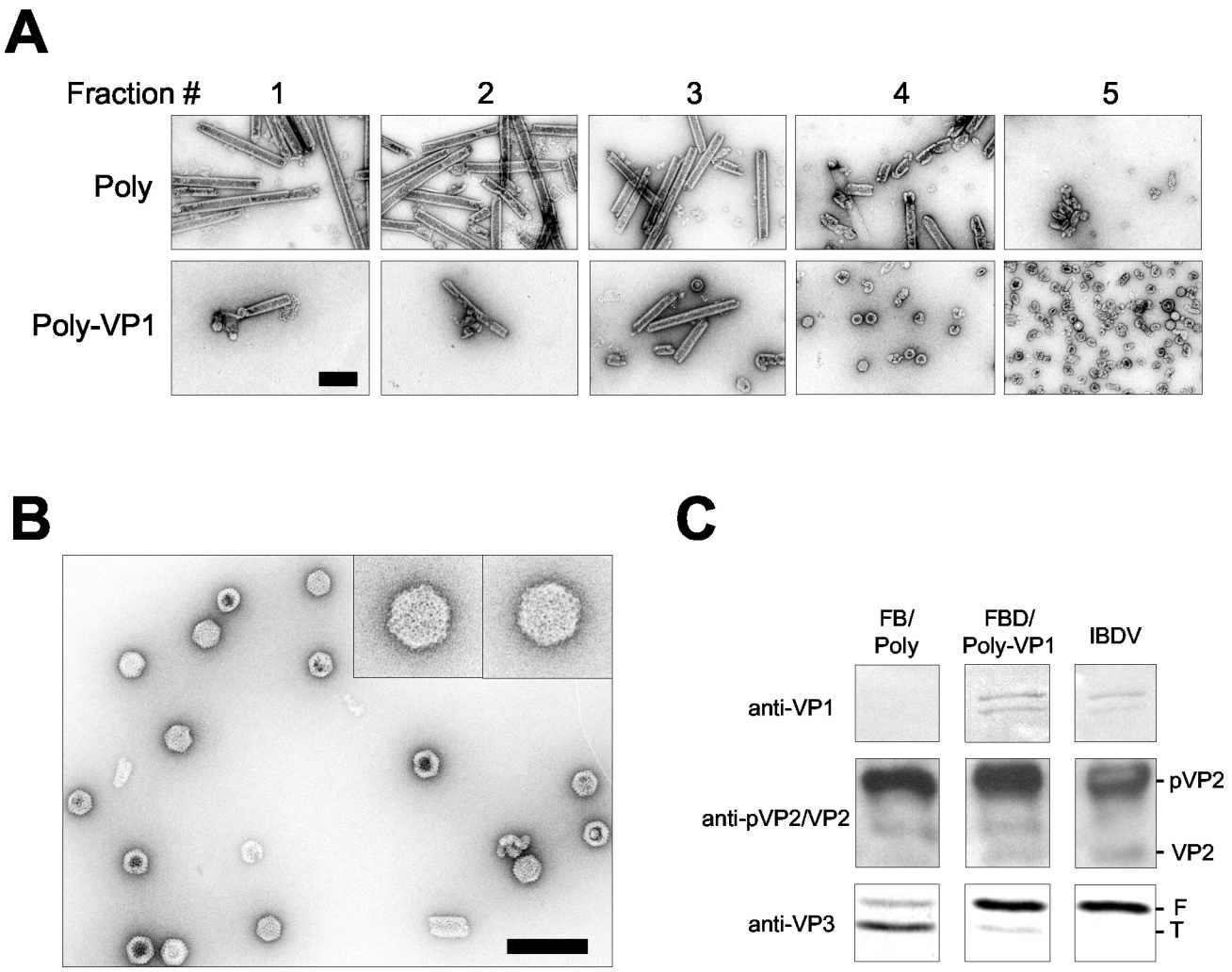

FIG. 9. Characterization of polyprotein-derived structures from cells infected with FBD/Poly-VP1. (A) H5 cells were infected with either FB/Poly or FBD/Poly-VP1. At 96 h postinfection, cells were harvested and lysed. Polyprotein-derived structures were purified by sedimentation in sucrose gradients. After centrifugation, six aliquots (2 ml/fraction) were collected, negatively stained with 2% uranyl acetate, and visualized by electron microscopy. Fraction 1 correspond to the bottom of the gradients. Fraction 6, containing soluble protein and disassembled structures, is not shown. Bar, 200 nm. (B) VLPs purified from FBD/Poly-VP1-infected cells. The electron microscopy image corresponds to fraction 5 from the FBD/Poly-VP1-derived gradient. Inlets show two VLPs at a higher magnification. Bar, 200 nm. (C) Characterization of polypeptides present in gradient fraction 5. An aliquot of fraction 5 from FB/Poly and FBD/Poly-VP1 was subjected to SDS-PAGE and Western blot with anti-VP1, anti-pVP2/VP2, and anti-VP3 sera. As a control, a sample from purified IBDV was used. The positions of pVP2, VP2, and full-length (F) and trimmed (T) VP3 are indicated.

diction results indicate that the highly charged C-terminal part of the protein (219 to 257) lacks a defined secondary structure because programs predict this region to be mainly in the coiled state (neither α nor β) with high reliability. The α-helical propensity of the C-terminal part of the protein (219 to 257) is very low (8%). A low-complexity region was found between positions 219 and 237. These regions usually are disordered (unstructured) (32). Actually, the PONDR system predicts a disordered segment between residues 222 and 239, with a score higher than 99%. The one-dimensional data indicate that the C-terminal VP3 region (from about residue 220) lacks a fixed three-dimensional structure, defined by secondary-structure elements in a given packing, but it is mainly unstructured and mobile.

DISCUSSION

Assembly of capsid proteins pVP2/VP2 and VP3 in IBDV-infected cells results in the formation of two well-differentiated structures, icosahedral capsids and tubular structures, known as type I tubules (18). In contrast, characterization of the structures produced upon polyprotein expression in insect cells has shown that, although accumulation of type I tubules is rather efficient, VLP production is almost null. Although several hypotheses have been suggested to explain this observation (26), a systematic investigation of this phenomenon has been lacking.

It has recently been described that insect cell expression of a chimerical polyprotein containing a C-terminal fusion to the

heterologous GFP results in the formation of bona fide IBDV VPLs (6). Polyprotein-GFP self-cleavage leads to accumulation of pVP2 and VP4 products, identical to those produced after expression of wild-type polyprotein, and a chimerical VP3-GFP fusion polypeptide. This was a strong hint that inefficient VLP assembly might be caused by an undefined disturbance of the VP3 physiological activity, prevented by fusing a globular polypeptide to its C-terminal end. Here, we show that expression of a polyprotein gene harboring a deletion in the VP3 coding sequence that removes the 105 C-terminal residues of the protein completely abolishes VLP production without affecting the assembly of type I tubules. These results revealed that VP3 plays a key role in VLP assembly. In addition, this finding also suggested that the inefficient VLP formation in insect cells might be due to an improper VP3 activity.

VP3 proteolysis. Analysis of polypeptide products generated upon polyprotein expression in insect cells showed the accumulation of two VP3 species with different electrophoretic mobilities: a 29-kDa product (VP3F), identical to that found in IBDV-infected cells; and a 27-kDa product (VP3T), produced by proteolytic cleavage at the C-terminal end of the protein. Time course expression analyses have shown that the VP3T/VP3F ratio increases with time. Indeed, at late times postinfection (72 to 96 h) VP3T constitutes the great majority of the total VP3 found in FB/Poly-infected insect cells. An identical phenomenon was observed after expression of His-VP3, a six-histidine-tagged version of VP3. Interestingly, the 27-kDa VP3T product was previously detected in both H5 and Sf9 cells infected with FastBac- and AcYM1-derived rBV vectors expressing the IBDV polyprotein (26). This polypeptide was considered an irrelevant VP3 degradation product (26).

Results presented here, obtained by Western blot analyses of IMAC-purified C-terminal His-VP3 deletion mutant proteins and mass spectrometry analysis of IMAC-purified His-VP3F and His-VP3T, showed that proteolytic cleavage removes a 13-amino-acid peptide from the VP3 C-terminal end. Hence, cleavage occurs between residues L244 and G245. According to the one-dimensional structure prediction, the scissile bond is located within a flexible and highly charged region. These two features have been associated with an increased susceptibility to proteolysis (29, 30). A mutational analysis around the scissile bond is currently ongoing. This might allow the construction of a polyprotein gene encoding a VP3 polypeptide unsusceptible to cleavage without compromising its functionality in insect cells. It is difficult to speculate about the reasons underlying the higher sensitivity of VP3 to proteolysis when expressed in insect cells. Degradation of proteins expressed in insect cells with rBVs has been reported frequently (17, 34, 39). VP3 C-terminal trimming might be caused by a protease of either cellular or viral origin.

It is noteworthy that accumulation of three VP3 species of approximately 29, 27, and 26 kDa early after IBDV infection has also been reported (38). Pulse-chase analysis indicated that the 27- and 26-kDa VP3 species are most likely generated by proteolytic processing of full-length VP3 (38). It would be interesting to determine whether these VP3-derived products are also generated by proteolysis of the C-terminal tail as well as to analyze their possible role during the virus replication cycle.

Coexpression of VP1 prevents VP3 trimming and restores VLP formation in insect cells. Formation of VP3-VP1 complexes has been characterized with both rVV vectors and yeast two-hybrid expression systems (23, 25, 38). This interaction is an essential step for VP1 encapsidation (23). We have recently showed that fusion of the 16-amino-acid VP1 binding motif, found at the VP3 C-terminal residues, confers the ability to bind VP1 on a heterologous polypeptide (25). According to the structural prediction, the VP1 binding motif lies at the end of a disordered region that is readily accessible to proteases. It was therefore hypothesized that the formation of VP3-VP1 complexes might hinder the VP3 cleavage site, and thus protect the VP3 C-terminal tail against proteolysis. The results presented here fully confirmed this hypothesis. VP3-VP1 complexes are efficiently formed in insect cells, and most important, VP1 coexpression largely prevents VP3 proteolysis. It seems highly likely that fusing GFP to the VP3 C-terminal end mimics the protective effect caused by the interaction with VP1 (6).

Interestingly, confocal laser scanning microscopy revealed that VP1 coexpression also induces the formation of viroplasm-like immunofluorescence signal similar to those observed in IBDV-infected cells (24). The presence of viroplasm-like structures in cells infected with FBD/Poly-VP1 suggested that polyprotein-VP1 coexpression might lead to efficient VLP morphogenesis in insect cells. This was investigated by electron microscopy analysis of fractions collected from cell extracts subjected to sucrose density gradient centrifugation. Abundant particles 65 to 70 nm in diameter, showing a distinctive polygonal contour identical to that of rVV-derived VLPs and IBDV virions, were detected in fractions in the gradient corresponding to extracts from cells infected with FBD/Poly-VP1.

These results demonstrate that VLP formation is associated with a blockade of VP3F→VP3T conversion. The fact that VLP formation in mammalian cells is completely independent of VP1 expression strongly indicates that the VP1 requirement to produce VLPs in insect cells is strictly restricted to protecting the C-terminal end of VP3 and thus allowing the proper functioning of the protein.

VP3 guides capsid assembly. Previous data strongly suggested that VP3 is responsible for the formation and/or stabilization of the fivefold vertex, a crucial step for the bending of the pVP2/VP2 capsomere lattice into icosahedral capsids (26). The VLP surface contains a defined proportion of hexamers and pentamers formed by pVP2-VP2 trimers. In contrast, the surface of type I tubules is exclusively formed by hexamers of pVP2-VP2 trimers (26). The fact that accumulation of VP3T results in the exclusive formation of type I tubules strongly suggests that this form of the protein is unable to trigger the bending of the capsomere lattice. A common feature of scaffolding proteins is their ability to establish self-interactions that result in the formation of functional oligomers. Disruption of this ability by either deletion or site-directed mutagenesis arrests capsid formation (8, 28, 45). Tacken et al. showed the ability of VP3 to form self-complexes (38). However, the domain(s) involved in oligomerization was not mapped.

The formation of high-molecular-mass oligomers, detectable by SDS-PAGE analysis, allowed us to map the VP3 oligomerization domain within a 24-amino-acid stretch (residues 224 to 247) near the C-terminal end of the polypeptide. According to

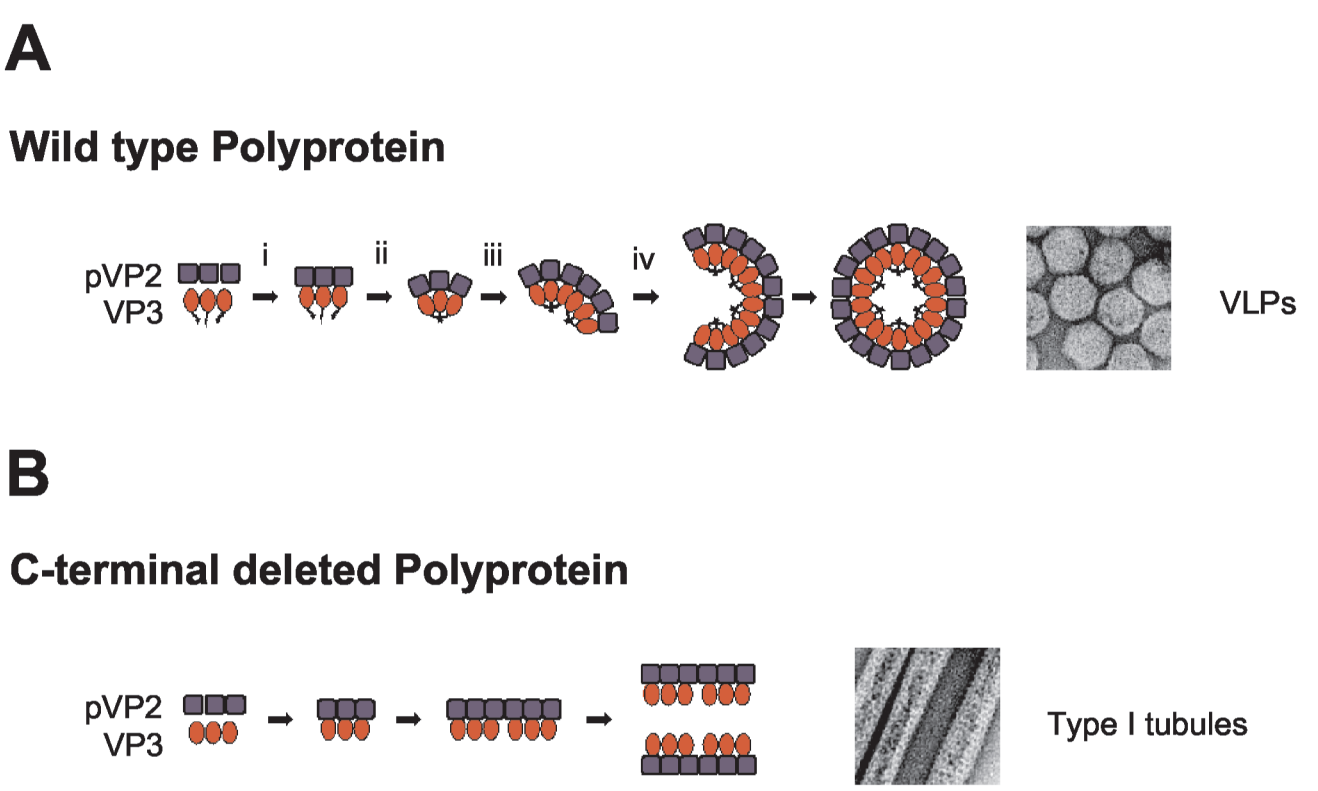

FIG. 10. VLP and type I tubule assembly models. (A) VLP assembly. (i) Polyprotein synthesis followed by self-cleavage releases the capsid proteins pVP2 and VP3; (ii) establishment of pVP2/VP3 interactions; (iii) VP3 oligomerization induces a series of conformational changes leading to bending of the pVP2 lattice and formation of fivefold vertexes; (iv) capsids are closed, generating mature VLPs. As has been suggested before, formation of fivefold vertexes and pVP→VP2 conversion might be tightly associated processes (6). (B) Formation of type I tubules. Deletion of the VP3 C-terminal end abrogates VP3 oligomerization, leading to the exclusive formation of type I tubules. Formation of type I tubules has also been observed in IBDV-infected cells as well as in cells infected with the virus expression vectors VT7/Poly and FBD/Poly-VP1, efficiently producing VLPs. It is unclear whether type I tubules in these cells represent intermediate assemblages involved in capsid formation or dead-end aberrant structures.

the one-dimensional structure prediction, the oligomerization domain maps within an unstructured protein domain. Unstructured protein regions are often associated with the formation of protein-protein complexes (11, 12). It has been shown that interactions through disordered regions, via a disorder-to-order transition, allow the affinity and specificity of the interactions to modulate (12). Additionally, the formation of these complexes often results in a conspicuous conformational change and consequently in an increased half-life of the complexed proteins (2, 43). It is tempting to speculate that the formation of VP3 self-complexes could lead to a conformational change(s) that would be transmitted to the interacting pVP2-VP2 trimeric capsomers, thus acting as a driving force for capsid morphogenesis.

Confocal laser scanning microscopy analysis of cells infected with VT7/PolyΔ907-1012, FB/PolyΔ1008-1012, FB/PolyΔ1003-1012, or FB/PolyΔ998-1012 showed that deletions affecting the VP3 oligomerization domain do not preclude VP3-pVP2 interaction. This demonstrates that VP3-pVP2 interaction and VP3 oligomerization are independent events and that the regions involved map within different protein domains. Data presented and discussed here allow the drawing of a simple working model (Fig. 10) describing a plausible sequence of events leading to IBDV VLP and type I tubule formation. At this point, it is difficult to determine whether type I tubules constitute intermediate assemblages in VLP morphogenesis or an aberrant structure, similar to those formed by capsid proteins from other viruses (7, 41). Work is in progress to shed light on this question.

ACKNOWLEDGMENTS

The first three authors contributed equally to the present work.

We thank Inés Poveda and Pilar Martínez for excellent graphic work, Silvia Gutierrez for advice and technical help on LCSM, and Emilio Camafeita and Juan P. Albar for mass spectrometry analyses. We also thank Daniel Luque, Juan R. Rodriguez, and Javier Ortego for critically reading the manuscript and for helpful advice.

Access to PONDR was provided by Molecular Kinetics (Pullman, Wash.) under license from the WSU Research Foundation.

This work was supported by grants BIO-2000-0905 from the Ministerio de Ciencia y Tecnología and 09/0043/2001 from the Subdirección General de Investigación of the Comunidad Autónoma de Madrid. A.M. and F.A. were recipients of fellowships from the Ministerio de Educación and the Subdirección General de Investigación of the Comunidad Autónoma de Madrid, respectively.

REFERENCES

1. **Altschul, S. F., W. Gish, W. Miller, E. W. Myers, and D. J. Lipman.** 1990. Basic local alignment search tool. J. Mol. Biol. **215:**403–410.
2. **Bell, S., C. Klein, L. Muller, S. Hansen, and J. Buchner.** 2002. p53 contains large unstructured regions in its native state. J. Mol. Biol. **322:**917–927.

3. **Birghan, C., E. Mundt, and A. E. Gorbalenya.** 2000. A non-canonical lon proteinase lacking the ATPase domain employs the ser-Lys catalytic dyad to exercise broad control over the life cycle of a double-stranded RNA virus. EMBO J. **19:**114–123.
4. **Bottcher, B., N. A. Kiselev, V. Y. Stel'Mashchuk, N. A. Perevozchikova, A. V. Borisov, and R. A. Crowther.** 1997. Three-dimensional structure of infectious bursal disease virus determined by electron cryomicroscopy. J. Virol. **71:**325–330.
5. **Castón, J. R., J. L. Martínez-Torrecuadrada, A. Maraver, E. Lombardo, J. F. Rodríguez, J. I. Casal, and J. L. Carrascosa.** 2001. C terminus of infectious bursal disease virus major capsid protein VP2 is involved in definition of the t number for capsid assembly. J. Virol. **75:**10815–10828.
6. **Chevalier, C., J. Lepault, I. Erk, B. Da Costa, and B. Delmas.** 2002. The maturation process of pVP2 requires assembly of infectious bursal disease virus capsids. J. Virol. **76:**2384–2392.
7. **Choi, J., and L. S. Loesch-Fries.** 1999. Effect of C-terminal mutations of alfalfa mosaic virus coat protein on dimer formation and assembly in vitro. Virology **260:**182–189.
8. **Cingolani, G., S. Moore, P. Prevelige, and J. Johnson.** 2002. Preliminary crystallographic analysis of the bacteriophage P22 portal protein. J. Struct Biol. **139:**46.
9. **Da Costa, B., C. Chevalier, C. Henry, J. C. Huet, S. Petit, J. Lepault, H. Boot, and B. Delmas.** 2002. The capsid of infectious bursal disease virus contains several small peptides arising from the maturation process of pVP2. J. Virol. **76:**2393–2402.
10. **Duncan, R., C. L. Mason, E. Nagy, J. A. Leong, and P. Dobos.** 1991. Sequence analysis of infectious pancreatic necrosis virus genome segment B and its encoded VP1 protein: a putative RNA-dependent RNA polymerase lacking the Gly-Asp-Asp motif. Virology **181:**541–552.
11. **Dunker, A. K., E. Garner, S. Guilliot, P. Romero, K. Albrecht, J. Hart, Z. Obradovic, C. Kissinger, and J. E. Villafranca.** 1998. Protein disorder and the evolution of molecular recognition: theory, predictions and observations. Pac. Symp. Biocomput. **3:**473–484.
12. **Dunker, A. K., J. D. Lawson, C. J. Brown, R. M. Williams, P. Romero, J. S. Oh, C. J. Oldfield, A. M. Campen, C. M. Ratliff, K. W. Hipps, J. Ausio, M. S. Nissen, R. Reeves, C. Kang, C. R. Kissinger, R. W. Bailey, M. D. Griswold, W. Chiu, E. C. Garner, and Z. Obradovic.** 2001. Intrinsically disordered protein. J. Mol. Graph. Model. **19:**26–59.
13. **Fernández-Arias, A., S. Martínez, and J. F. Rodríguez.** 1997. The major antigenic protein of infectious bursal disease virus, VP2, is an apoptotic inducer. J. Virol. **71:**8014–8018.
14. **Fernández-Arias, A., C. Risco, S. Martínez, J. P. Albar, and J. F. Rodríguez.** 1998. Expression of ORF A1 of infectious bursal disease virus results in the formation of virus-like particles. J. Gen. Virol. **79:**1047–1054.
15. **Grimes, J. M., J. N. Burroughs, P. Gouet, J. M. Diprose, R. Malby, S. Zientara, P. P. Mertens, and D. I. Stuart.** 1998. The atomic structure of the bluetongue virus core. Nature **395:**470–478.
16. **Jones, D. T.** 1999. Protein secondary structure prediction based on position-specific scoring matrices. J. Mol. Biol. **292:**195–202.
17. **Kadono-Okuda, K., M. Yamamoto, Y. Higashino, K. Taniai, Y. Kato, S. Chowdhury, J. Xu, S. K. Choi, M. Sugiyama, K. Nakashima, et al.** 1995. Baculovirus-mediated production of the human growth hormone in larvae of the silkworm, *Bombyx mori*. Biochem. Biophys. Res. Commun. **213:**389–396.
18. **Kaufer, I., and E. Weiss.** 1976. Electron-microscope studies on the pathogenesis of infectious bursal disease after intrabursal application of the causal virus. Avian Dis. **20:**483–495.
19. **Kochan, G. D. González, and J. F. Rodríguez.** 2003. Characterization of the RNA binding activity of VP3, a major structural protein of IBDV. Arch. Virol. **148:**723–744.
20. **Lacroix, E., A. R. Viguera, and L. Serrano.** 1998. Elucidating the folding problem of alpha-helices: local motifs, long-range electrostatics, ionic-strength dependence and prediction of NMR parameters. J. Mol. Biol. **284:**173–191.
21. **Lemon, M. K., D. H. L. Bishop, E. B. Carstens, M. K. Estes, C. M. Fauquet, D. J. McGeoch, J. Maniloff, M. A. Mayo, C. R. Pringle, R. B. Wickner, and M. H. B. van Regenmortel.** 2000. Virus taxonomy: seventh report of the International Committee on Taxonomy of Viruses. Academic Press, San Diego, Calif.
22. **Li, X., P. Romero, M. Rani, A. K. Dunker, and Z. Obradovic.** 1999. Predicting protein disorder for N-, C-, and internal regions. Genome Inform. Ser. Workshop Genome Inform. **10:**30–40.
23. **Lombardo, E., A. Maraver, J. R. Castón, J. Rivera, A. Fernández-Arias, A. Serrano, J. L. Carrascosa, and J. F. Rodríguez.** 1999. VP1, the putative RNA-dependent RNA polymerase of infectious bursal disease virus, forms complexes with the capsid protein VP3, leading to efficient encapsidation into virus-like particles. J. Virol. **73:**6973–6983.
24. **Lombardo, E., A. Maraver, I. Espinosa, A. Fernández-Arias, and J. F. Rodríguez.** 2000. VP5, the nonstructural polypeptide of infectious bursal disease virus, accumulates within the host plasma membrane and induces cell lysis. Virology **277:**345–357.
25. **Maraver, A., R. Clemente, J. F. Rodríguez, and E. Lombardo.** Identification and molecular characterization of the RNA polymerase-binding motif of the inner capsid protein VP3 of infectious bursal disease virus. J. Virol. **77:**2459–2468.
26. **Martínez-Torrecuadrada, J. L., J. R. Castón, M. Castro, J. L. Carrascosa, J. F. Rodríguez, and J. I. Casal.** 2000. Different architectures in the assembly of infectious bursal disease virus capsid proteins expressed in insect cells. Virology **278:**322–331.
27. **Prasad, B. V., R. Rothnagel, C. Q. Zeng, J. Jakana, J. A. Lawton, W. Chiu, and M. K. Estes.** 1996. Visualization of ordered genomic RNA and localization of transcriptional complexes in rotavirus. Nature **382:**471–473.
28. **Preston, V. G., and I. M. McDougall.** 2002. Regions of the herpes simplex virus scaffolding protein that are important for intermolecular self-interaction. J. Virol. **76:**673–687.
29. **Realini, C., S. W. Rogers, and M. Rechsteiner.** 1994. KEKE motifs. Proposed roles in protein-protein association and presentation of peptides by MHC class I receptors. FEBS Lett. **348:**109–113.
30. **Rechsteiner, M., and S. W. Rogers.** 1996. PEST sequences and regulation by proteolysis. Trends Biochem. Sci. **21:**267–271.
31. **Reinisch, K. M., M. L. Nibert, and S. C. Harrison.** 2000. Structure of the reovirus core at 3.6 A resolution. Nature **404:**960–967.
32. **Romero, P., Z. Obradovic, X. Li, E. C. Garner, C. J. Brown, and A. K. Dunker.** 2001. Sequence complexity of disordered protein. Proteins. **42:**38–48.
33. **Rost, B.** 1996. PHD: predicting one-dimensional protein structure by profile-based neural networks. Methods Enzymol. **266:**525–539.
34. **Sakurai, T., Y. Ueda, M. Sato, and A. Yanai.** 1992. Feline interferon production in silkworm by recombinant baculovirus. J. Vet. Med. Sci. **54:**563–565.
35. **Sánchez, A. B.** 2000. Ph.D. thesis. Universidad Autónoma de Madrid, Madrid, Spain.
36. **Sánchez, A. B., and J. F. Rodriguez.** 1999. Proteolytic processing in infectious bursal disease virus: identification of the polyprotein cleavage sites by site-directed mutagenesis. Virology **262:**190–199.
37. **Sharma, J. M., I. J. Kim, S. Rautenschlein, and H. Y. Yeh.** 2000. Infectious bursal disease virus of chickens: pathogenesis and immunosuppression. Dev. Comp. Immunol. **24:**223–235.
38. **Tacken, M. G., P. J. Rottier, A. L. Gielkens, and B. P. Peeters.** 2000. Interactions in vivo between the proteins of infectious bursal disease virus: capsid protein VP3 interacts with the RNA-dependent RNA polymerase, VP1. J. Gen. Virol. **81:**209–218.
39. **Takahashi, S., S. Ushiyama, T. Suzuki, K. Ogawa, and K. Oda.** 1997. Purification and characterization of cysteine proteinase from a baculovirus gene. Biosci. Biotechnol. Biochem. **61:**1507–1511.
40. **van den Berg, T. P., N. Eterradossi, D. Toquin, and G. Meulemans.** 2000. Infectious bursal disease (Gumboro disease). Rev. Sci. Technol. **19:**509–543.
41. **Volpers, C., P. Schirmacher, R. E. Streeck, and M. Sapp.** 1994. Assembly of the major and the minor capsid protein of human papillomavirus type 33 into virus-like particles and tubular structures in insect cells. Virology **200:**504–512.
42. **Wootton, J. C., and S. Federhen.** 1996. Analysis of compositionally biased regions in sequence databases. Methods Enzymol. **266:**554–571.
43. **Wright, P. E., and H. J. Dyson.** 1999. Intrinsically unstructured proteins: reassessing the protein structure-function paradigm. J. Mol. Biol. **293:**321–331.
44. **Yao, K., and V. N. Vakharia.** 2001. Induction of apoptosis in vitro by the 17-kDa nonstructural protein of infectious bursal disease virus: possible role in viral pathogenesis. Virology **285:**50–58.
45. **Zhou, Z. H., S. J. Macnab, J. Jakana, L. R. Scott, W. Chiu, and F. J. Rixon.** 1998. Identification of the sites of interaction between the scaffold and outer shell in herpes simplex virus-1 capsids by difference electron imaging. Proc. Natl. Acad. Sci. USA **95:**2778–2783.